Engineering Structures 226 (2021) 111351

Contents lists available at ScienceDirect

Engineering Structures

journal homepage: www.elsevier.com/locate/engstruct

Experimental and numerical analysis of mounting force of auxetic dowels for furniture joints

Tolga Kuşkun [a], Jerzy Smardzewski [b,*], Ali Kasal [a]

[a] Department of Woodworking Industrial Engineering, Faculty of Technology, Muğla Sıtkı Koçman University, Muğla, Turkey
[b] Poznan University of Life Sciences, Faculty of Wood Technology, Department of Furniture Design, Wojska Polskiego 28, 60-637 Poznan, Poland

ARTICLE INFO

Keywords:
Auxetic
Dowel
Mounting force
Friction
Contact pressure
FEM

ABSTRACT

Limited number of papers describe the practical use of auxetics in the wood and furniture sector. Only one paper describes the auxetic nails. None of them analyzed the impact of using auxetics on the strength of furniture joints. The aim of this investigation was to design and manufacture different kinds of auxetic dowels with corresponding muffs and experimentally, theoretically, and numerically analyze the minimum mounting forces, contact pressures, and friction coefficients of these dowels in particleboard. Firstly, auxetic properties of the dowels were numerically determined, and then obtained values were confirmed by real compression tests in order to be sure that the dowels had negative Poisson's ratios. All dowels were manufactured from polyamide (PA12) with 3D printing Selective Laser Sintering (SLS) technology. Static compression tests were carried out for obtaining the minimum mounting force needed to insert the dowel into the muff. Numerical analyses were performed by means of Abaqus/Explicit v6.14-2 software. Contact pressures and friction coefficients were also theoretically calculated and compared to the results of numerical analyses and real tests. At the end of the tests, the auxetic dowels gave lower mounting force values than the non-auxetic dowels. Mounting force values of dowels decreased as the dowel hole diameter and size of inclusions are increased. Furthermore, the contact pressures on the surface of the auxetic dowels were considerably lower than in the non-auxetic dowels. In conclusion, it could be said that the auxetic dowels could be utilized as an alternative fastener for the traditional furniture dowels. Therefore, withdrawal strength and corner joint tests of the auxetic dowels should be investigated in future studies.

1. Introduction

Today, conventional materials are generally used in engineering, manufacturing, and especially in the production of mechanical fasteners for furniture joints. However, the interest and need for smart metamaterials are increasing day by day, which encourages the design, production, and use of new alternative materials. Smart material designs and productions are made either by developing a new product or by adding extra properties to the traditional materials.

A material's Poisson's ratio reflects the deformation of its cross-section in response to an orthogonal tensile strain. Models of structures with a negative Poisson's ratio were described as early as 30 years ago [1–3]. They were made in 1987 by Lakes [4], and called auxetics by Evans [5]. Over these past thirty years, studies on auxetics diverge into different aspects. Over these past thirty years, the studies on auxetic materials and structures presented different theoretical and practical aspects. Among others, the search for auxetic properties in new materials [6,7], the theoretical studies of various models exhibiting auxetic properties [8–21], or the creation of auxetic composites in order to enhance mechanical properties of materials [22,23]. The latter is of particular importance if one considers practical applications of negative Poisson's ratio materials [24–27]. Auxetic materials and structures are expected to have many desirable mechanical properties such as shear resistance, indentation resistance, synclastic behavior [28,29]variable permeability, high energy absorption, and fracture resistance. Auxetics may be useful in applications such as body armor, packing material, knee and elbow pads, robust shock-absorbing material, and sponge mops. These materials have been shown to possess enhanced hardness and toughness, as well as absorb vibrations and sound better than their non-auxetic counterparts [30,31]. The atypical elastic behavior of auxetic materials is enabling advancements in a broad range of technologies such as impact-resistant composites, extremely precise sensors,

* Corresponding author.
E-mail addresses: tolgakuskun@mu.edu.tr (T. Kuşkun), jsmardzewski@up.poznan.pl (J. Smardzewski), alikasal@mu.edu.tr (A. Kasal).

https://doi.org/10.1016/j.engstruct.2020.111351
Received 24 February 2020; Received in revised form 13 September 2020; Accepted 18 September 2020
Available online 10 October 2020

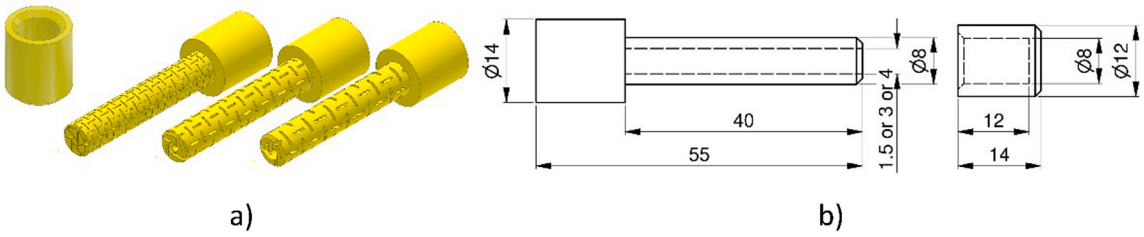

Fig. 1. General view of the dowel and muff: (a) shape, (b) dimensions.

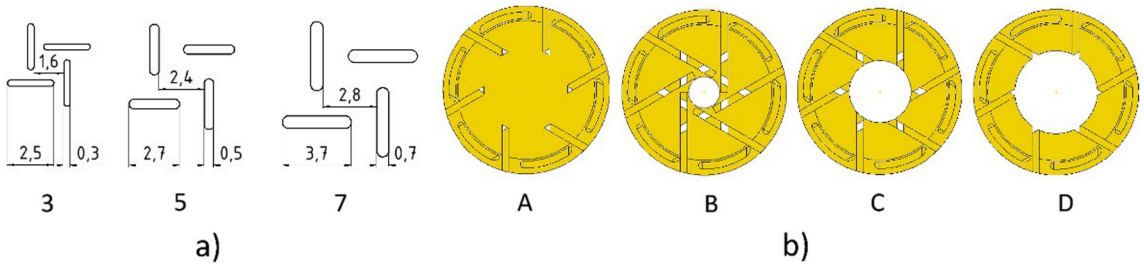

Fig. 2. Dimensions (in mm) of auxetic inclusion (a) and cross-sectional geometries (b) of dowels.

tougher ceramics, and high-performance armor [29,32]. Santulli and Langella [33] discussed the experience of using auxetic materials in different design objects including chairs, bags, seat belts, etc. Structures were calculated and modelled as chiral with defined geometrical parameters and then applied to concepts with the fabrication of real models using neoprene or generally rubbery material.

The interest in auxetic materials has been increasing in recent years, so studies based on the experimental and modeling for these materials are becoming widespread. In contrast to aviation, shipbuilding, and automotive industry, only a few reports concern the application of auxetics in the wood and furniture industry [34–39]. The authors described that layered wood-based sandwich panels are an excellent alternative for comparable composites manufactured from metals or plastics. They are lighter, and in relation to their density, they are more rigid and stronger. This facilitates the efficient management of natural resources since they are derived from renewable materials. A limited number of papers also describe the practical use of auxetics in furniture design. The aim of the studies carried by the Smardzewski et al. [40,41] was to develop a model of an auxetic compression spring useful in seat constructions of office and home furniture. In the case of furniture joints, auxetics has not yet been used. Under uniaxial compression (tension), auxetic materials would shrink (expand) laterally. In the study carried by Ren et al. [26], the first auxetic nails are designed, fabricated and experimentally investigated. Pine timber and medium-density fiberboard are selected as testing materials. The push-in and pull-out performance of auxetic and non-auxetic nails is compared by using two key parameters of the maximum compressive force and the maximum tensile force. It is found that the auxetic nails do not always exhibit superior mechanical performance to non-auxetic ones. Also, the small auxetic deformation of one typical designed auxetic nail is revealed by the experimentally validated finite element model. The experimental and numerical results illustrate the limitations of exploiting the auxetic property in the nail application. Some suggestions are provided for more effective designs of future auxetic nails.

Nails, however, have no application in the design of contemporary furniture, especially wooden and undemountable (glued) furniture. Most common application in the furniture industry is wooden dowels glued into the holes with the use of glue. The holes have larger diameters than the dowels. Such a loose fit allows the application of glue into the holes and mounting of the dowels. The formed shape-adhesive joints are undemountable and used for the assembly of furniture delivered to end-users in full. The withdrawal strength of the dowels depends on many factors. Uysal [42] showed that laminated beech veneer dowels gave higher withdrawal force from medium density fibreboards than from particleboard. Erdil et al. [43] and Cha [44] determined that the withdrawal strength of dowels depends on the diameter of the dowel and hole. This study indicated that dowel withdrawal strength increase in a linear fashion as a gap between dowel and hole decreases. Yapici et al.

Table 1
Dowel types designed, manufactured and tested in this study.

Dowel type	Hole type	Inclusion size	Average diameter of dowels (mm)	Average inner diameter of muffs (mm)	Average interference tolerance (mm)	Dowel code
Non-auxetic	RF	Plain	7.86	7.59	+0.27	RF
Auxetic	A	3	7.88	7.50	+0.38	A3
		5	7.91	7.56	+0.35	A5
		7	7.90	7.56	+0.34	A7
	B	3	7.89	7.52	+0.37	B3
		5	7.89	7.54	+0.35	B5
		7	7.89	7.49	+0.39	B7
	C	3	7.87	7.56	+0.31	C3
		5	7.87	7.58	+0.29	C5
		7	7.86	7.52	+0.35	C7
	D	3	7.84	7.54	+0.30	D3
		5	7.86	7.59	+0.27	D5
		7	7.87	7.55	+0.32	D7

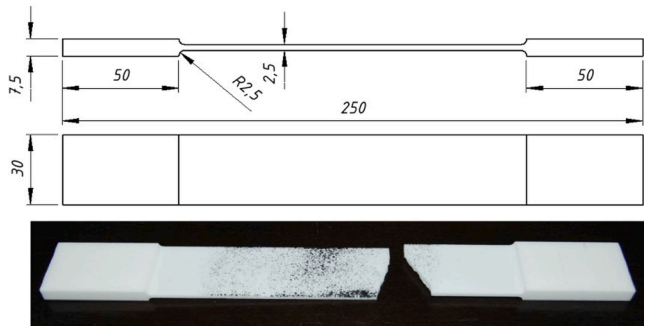

Fig. 3. Front and side views and real picture of the static tensile test samples.

[45] determined the withdrawal strengths of 6, 8, 10 mm diameter dowels produced from beech with respect to the edge of medium-density fiberboard (MDF) or particleboard edged with 5, 10, and 15 mm thickness of solid wood edge banding of scotch pine, oriental beech and lime tree, bonded with hot-melt, poly (vinyl acetate) (PVAc) and Desmodur-VTKA (D-VTKA), a polyurethane-based one-component adhesive. The highest withdrawal strength was obtained in beech dowels with 8 mm diameter for MDF with 5 mm thickness of solid wood edge banding of bonded beech with D-VTKA adhesive. Özcan et al. [46] determined that the strength of dowels pulling out of narrow surfaces of furniture elements made of various types of wood, and glued by PVAc and D-VTKA. Eckelman and Cassens [47] indicated that plain dowels and spiral-grooved dowels with fine grooving give greater withdrawal strength from the face of particleboard than do multigroove dowels at least when excess adhesive is applied in the holes and subsequently forced into the substrate as the dowels are inserted into the holes. Erdil and Eckelman [48] developed predictive expressions that allow designers to estimate withdrawal strength as a function of the diameter of dowels, their depth of embedment, and density of the composite material. The quantitative effect of dowel dimension, dowel position, and loading distance on bending moment capacity was studied in the paper [49]. The results showed that the neutral line position keeps almost steady with various dowel spaces for the two-pin joint. Increasing dowel diameter and length, fortifying dowel rupture and withdrawal strength, enlarging dowel space, or moving the bottom dowel far away from the bottom edge will promote the joint performance.

The above studies prove that, despite their high popularity and low production costs, the dowel joints are not easy to use optimally. Their strength depends on many factors. From a practical point of view, for the end-user, they constitute a significant difficulty in assembling the furniture. The application of glue and the need to maintain pressure for a long time during assembly discourage manufacturers from using these solutions for ready-to-assemble (RTA) furniture. Dowels with auxetic structure do not require glue during the application. They decrease in diameter when compressed and increase in diameter when stretched. Therefore, they can be an alternative to dowel joints in undemountable furniture.

As seen in reviewed literature, there are many studies related to the auxetic materials, however, the studies on application of the auxetic materials in furniture joints are very limited. Specifically, it was considered in the current study that the auxetic property could be used to design various superior dowels for easier push–in and harder pull–out in order to utilize in the furniture joints. The designed dowels could be utilized for one–time ready to assemble (RTA) furniture joints; therefore, determining the minimum mounting forces required for assembling the

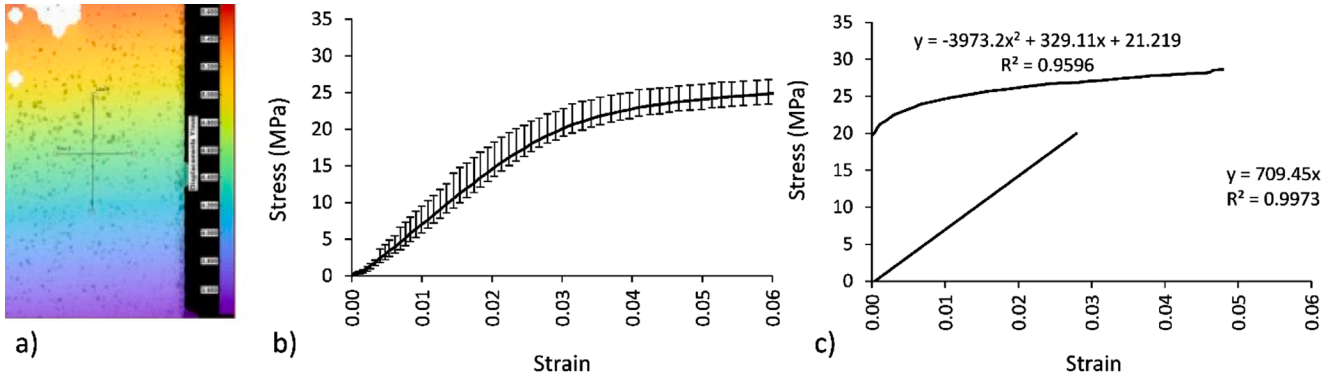

Fig. 4. Pattern matching method and stress–strain relationship for PA12: (a) virtual gauges, (b) original curve from the experiment, (c) converted stress–strain relationship.

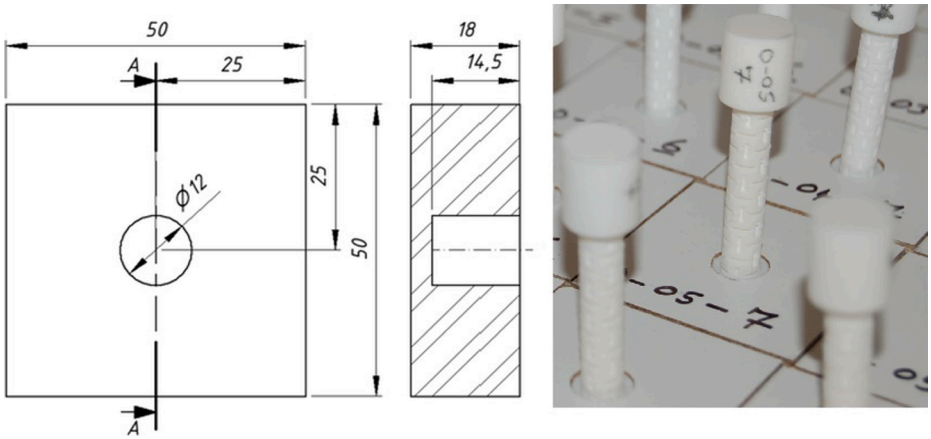

Fig. 5. Dimensions and general configuration of samples.

furniture joints are very important.

Advanced 3D printing techniques may prove useful in such prototype studies. Application of the Selective Laser Sintering (SLS) technology makes it possible to construct even highly complex prototypes of joints of a high degree of isotropy in the used material.

In this context, designing, producing and evaluating the strength of fasteners used in the furniture joints with auxetic materials was found worthy of research. Accordingly, the aim of this study was to design and manufacture different kinds of auxetic dowels with corresponding muffs in 3D printing technology, and experimentally, theoretically, and numerically analyze the minimum mounting forces, contact pressures and friction coefficients of these dowels in particleboard.

2. Materials and methods

2.1. Design and manufacturing of auxetic dowels and muffs

In the scope of study, 12 types of auxetic dowels with different patterns, and a non-auxetic dowel, and corresponding muffs were evaluated. All dowels designed were in 40 mm length and 8 mm diameter; while the corresponding muffs were in 14 mm length and 12 mm diameter (Fig. 1). On the outside surface of dowels three type (3, 5, 7) of rectangular inclusions (rectangles with semicircles in two ends) were prepared (Fig. 2a). The dowel core was made as full (A) or with a 1.5 mm, 3 mm and 4 mm hole marked in Fig. 1b as B, C, D, respectively.

The inclusion size factor (3, 5, 7) is described as the thickness of the 4 rectangles that create the rectangular pattern. All the other dimensions are depending on the thickness of these rectangles. The pattern on the whole dowel surface consists of repeating the 4 rectangular inclusions in the longitudinal and circumferential directions. For the comparison, a non-auxetic dowel without a hole was designed as a reference dowel (RF). All manufactured dowels had a special head for easy application of the mounting force. Totally, 130 dowels, including 13 different types of dowels and 10 repetitions for each, were manufactured for this study. The experimental design of the study is presented in Table 1.

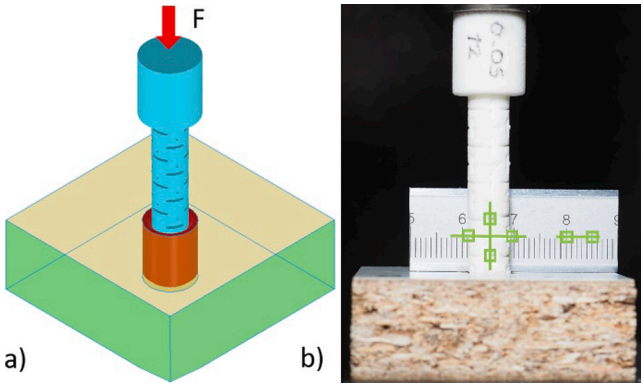

Fig. 6. The geometry of samples for mounting tests: (a) loading, (b) measuring of strains.

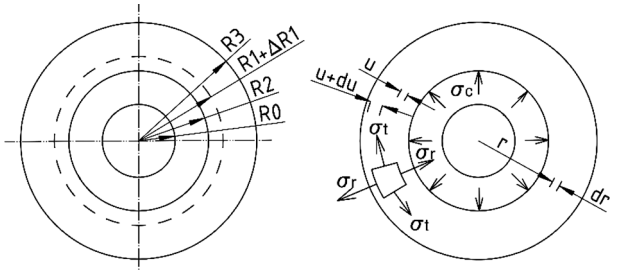

Fig. 7. Model of the pressed joint with dowels and hole.

It should be noted that most of the parameters were selected due to the manufacturing capacity of the 3D printing machine Lisa Sinterit, (3D Center, Wrocław, Poland). Firstly, 3D models of the designed dowels were modeled in the Autodesk Inventor software (Autodesk, Warszawa, Polska). Then, based on the CAD models, STP and STL models were prepared for numerical calculations and 3D printing, respectively. The designed dowels were printed by using polyamide (PA12) (3D Center, Wrocław, Poland).

2.2. Materials

The mechanical and elastic properties of the PA12 were determined according to the uniaxial static tensile tests in accordance with the procedures described in ASTM D3039/D3039M–17 [50]. The 3D printed tensile test sample is shown in Fig. 3. A total of 10 samples were prepared.

Uniaxial tensile tests were carried out on a 10 kN capacity numerically controlled Zwick 1445 universal testing machine (Zwick Roell AG, Ulm, Germany) with a 10 mm/min loading rate under the static loads. Elongations and shortenings in the middle part of the samples subjected to tension were recorded by Digital Image Correlation and Tracking method (DICT) using Dantec system (Dantec Dynamics A/S, Skovlunde, Denmark) (Fig. 4a). In order to include plasticity in numerical calculations for selected dowels, the experimental stress–strain dependence (Fig. 4b) had to be converted for polyamide (PA12) after the linear elastic range was exceeded (Fig. 4c). First the linear elastic range was determined establishing the linear equation for this section. As shown in Fig. 4b, the slope of the straight line corresponds to the value of the modulus of linear elasticity for polyamide equal to $E = 709$ (standard deviation $SD = 41$) MPa, tensile strength $MOR = 41$ MPa ($SD = 3.5$ MPa), Poisson's ratio $\upsilon = 0.23$ ($SD = 0.01$). Next true stress σ_T and the logarithmic plastic strain ε_L, required in the FEM algorithm, were calculated using the equations given below:

$$\varepsilon_L = \varepsilon_T - \left(\frac{\sigma_T}{E_L}\right) \tag{1}$$

where $\sigma_T = \sigma(1+\varepsilon)$, true stress, $\varepsilon_T = ln(1+\varepsilon)$ logarithmic strain, $E =$

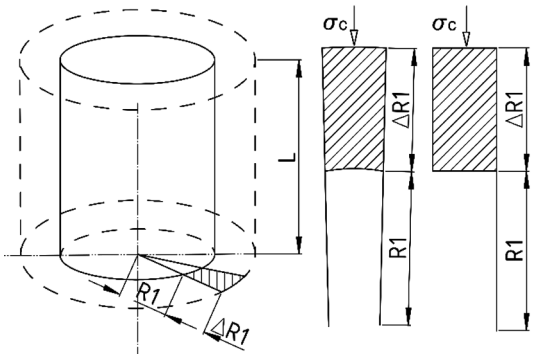

Fig. 8. Model of the pressed joint with dowels without hole.

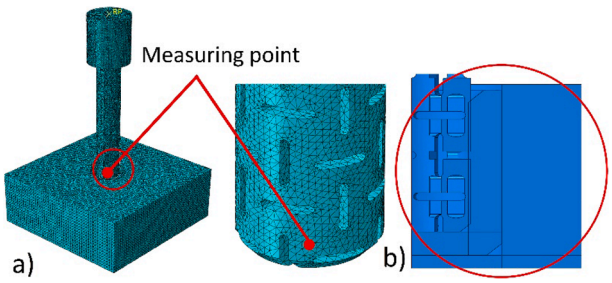

Fig. 9. Mesh model of mounting force samples and measuring point.

modulus of elasticity of polyamide, σ = engineering stress, and ε = engineering strain. For the plastic range in Fig. 4b above the straight line, the graph for $\sigma_T = f(\varepsilon_L)$ was plotted.

The sample base was made of particle board 18 mm in thick, modulus of elasticity MOE = 2488 MPa (SD = 43 MPa), modulus of rupture MOR = 11.17 MPa (SD = 1.25 MPa, υ = 0.30). The muffs were glued to the particleboards using Jowat® UniPUR 687.22 adhesive (Jowat Swiss AG, Buchrain, Swissland). Totally, 130 mounting force test samples were prepared and tested. Before the tests, diameter of dowels and inner diameter of corresponding muffs were individually measured with a digital caliper. On this base, the average interference tolerance was calculated (Table 1). These data were used in numerical and theoretical calculations of contact pressure between dowels and muffs. Then samples were kept for two weeks in a conditioning chamber at 20 °C ± 2 °C and 65% ± 3% relative humidity. The dimensions and general view of mounting force sample is shown in Fig. 5.

3. Experiment

All of the mounting force test of the dowels were carried out on a 10 kN capacity numerically controlled Zwick 1445 universal testing machine (Zwick Roell AG, Ulm, Germany) with a 10 mm/min loading rate under the static uniaxial loading (Fig. 6a). In the tests, dowels were inserted into the muff on the 10 mm deep during the time period 60–90 s. The mounting forces F (N) needed to insert the dowel into the muff and corresponding displacements were recorded with accuracy 0.01 N and 0.01 mm respectively. On this basis, the influence of the type of dowel on the value of mounting force were determined.

In the mounting force tests; in order to obtain the Poisson's ratio of dowels, a reference ruler was placed behind the specimens. Before and during the loading, a few pictures of the samples were taken with an Olympus OM-D camera (Olympus, Tokyo, Japan). Next dowel strains in vertical and horizontal directions were analyzed using the National Instruments IMAQ Vision Builder 6.1 linear analysis software (National Instruments, Texas, USA) (Fig. 6b). Applying the edge detection method in the digital image analysis, Poisson's ratios were calculated. The methodology of calculating the Poisson's ratios using digital image analysis was detailed described in previous publications [51–53]. The edges of the inclusions located along the axis of the dowel were selected as the vertical characteristic points. In the direction of the dowel diameter, the characteristic points were the line of the side wall of the dowel, clearly visible in the black and white pictures. For each type of dowel 10 replications was used. In total, 130 mounting force tests were performed. In accordance with the method used, the coefficients were determined for the range of linear elasticity. Therefore, it was assumed that their values would be statistically constant in this range.

4. Theoretical model of contact

To determine the contact pressures in the pressed joint (in this case mounting force samples), the *Lame* analogy was used [54]. In the analyzed case, the muff has an outer radius R_3 (mm) and an inner radius R_2 (mm) (Fig. 7). The dowel has an outer radius $R_1 + \Delta R_1$ (mm), larger by ΔR_1 (mm) than the inner radius of the muff R_2, and the radius of the central hole R_0 (mm).

The process of mounting the connection is equivalent to exerting contact stress (pressure) σ_c (MPa) on the inner surface of the muff and the same stress on the outer surface of the dowel. The value of this stress was calculated from the assumption that $R_1 = R_2$ due to the contact stress σ_c. Using the solution proposed by Lipka [54]circumferential stresses σ_t (MPa) and radial stresses σ_r(MPa) in the elementary segment of the muff can be expressed in the form:

$$\sigma_t = \frac{E}{1-\vartheta^2}\left(\frac{u}{r} + \vartheta\frac{du}{dr}\right) \tag{2}$$

$$\sigma_r = \frac{E}{1-\vartheta^2}\left(\frac{du}{dr} + \vartheta\frac{u}{r}\right) \tag{3}$$

where: E (MPa) – dowel module of elasticity, ϑ – Poissons ratio, du (mm) – increment of displacement in the radius direction, u (mm) – displacement in the radius direction, dr (mm) – increment of intermediate radius, u (mm) – intermediate radius. For the connection as in the Fig. 7, the appropriate stresses can be presented by *Lame* equations [54]:

$$\sigma_t = \frac{\sigma_c R_2^2}{R_3^2 - R_2^2}\left(1 + \frac{R_3^2}{r^2}\right) - \frac{\sigma_c R_3^2}{R_3^2 - R_2^2}\left(1 + \frac{R_2^2}{r^2}\right) \tag{4}$$

$$\sigma_r = \frac{\sigma_c R_2^2}{R_3^2 - R_2^2}\left(1 - \frac{R_3^2}{r^2}\right) - \frac{\sigma_c R_3^2}{R_3^2 - R_2^2}\left(1 - \frac{R_2^2}{r^2}\right) \tag{5}$$

hence the new outer radius of the dowel R_1 taking into account the displacement u for $r = R_1$ is equal to:

$$R_1 + \Delta R_1 + u_{r=R_1} = R_1 + \Delta R_1 - \frac{\sigma_c R_1}{E}\left(\frac{R_1^2 + R_0^2}{R_1^2 - R_0^2} - \vartheta\right) \tag{6}$$

and inner radius of the muff R_2 , taking into account the displacement u for $r = R_1$ is equal to:

$$R_2 = R_1 + u_{r=R_1} = R_1 + \frac{\sigma_c R_1}{E}\left(\frac{R_3^2 + R_1^2}{R_3^2 - R_1^2} + \vartheta\right) \tag{7}$$

Therefore, after comparing Eqs. (6) and (7), it can be obtained the value of contact pressures in the pressed joint:

$$\sigma_c = \frac{E\Delta R_1}{2R_1^3}\left(\frac{\left(R_3^2 - R_1^2\right)\left(R_1^2 - R_0^2\right)}{R_3^2 - R_0^2}\right) \tag{8}$$

In the case of a joint in which the dowel has no hole, it can be applied classic Hook's law. Hence, using the markings as in the Fig. 8 and replacing the angular segment of the circle with a rectangular segment, contact pressures can be written in the form:

$$\sigma_c = \frac{\Delta R_1}{R_1 + \Delta R_1}E \tag{9}$$

Therefore the mounting force F (N) can be calculated taking into account the friction coefficient μ:

Table 2
Poisson's ratio values of the dowels from numerical analyses and experiment.

Dowel type	Dowel code	Numerical analyses (ϑ_n)	Experiment (ϑ_t)
Non-auxetic	RF	0.219	0.230
	A3	0.217	0.227
	A5	0.207	0.214
	A7	0.146	0.133
Auxetic	B3	−0.147	−0.153
	B5	−0.213	−0.201
	B7	−0.234	−0.256
	C3	−0.185	−0.182
	C5	−0.236	−0.229
	C7	−0.311	−0.346
	D3	−0.336	−0.357
	D5	−0.377	−0.388
	D7	−0.412	−0.442

Table 3
Summary of ANOVA results for mounting forces according to first approach.

Source	Degrees of freedom	Sum of squares	Mean squares	F–Value	P–Value
Dowel type	12	673,810	56150.8	73.26	0.000
Error	117	89,675	766.5		
Total	129	763,484			

Table 4
Mean mounting force F (N) of the dowels with their coefficients of variation.*

Dowel type	RF	A3	A5	A7	B3	B5	B7	C3	C5	C7	D3	D5	D7
Mean (N)	290	252	302	231	211	236	194	96	151	127	88	122	100
COV* (%)	18.4	10.8	11.0	15.3	14.3	16.6	9.4	18.7	9.4	11.5	14.7	11.8	9.6
HG	A	B	A	BC	CD	B	D	H	E	EF	H	FG	GH

* Values followed by the same capital letter are not significantly different, COV: Coefficients of variation.

$$F = 2\mu\sigma_c\pi R_1 L \tag{10}$$

where: L (mm) – the length of the dowel in the muff.

In the planned task, the mounting force F was experimentally determined first. Then the contact pressure value was calculated numerically σ_c. On this basis, the coefficients of friction for individual types of connections were calculated from the equations:

$$\mu = \frac{F}{2\sigma_c\pi R_1 L} \tag{11}$$

5. Numerical model

Models of samples were supported analogy as in the experimental part. Geometry, loading and boundary conditions of the model were based on Fig. 6. In general, 10-node modified quadratic tetrahedron element C3D10M type, was used to all parts of model (about 657,000 elements and 1,622,000 nodes per model) (Fig. 9a). As shown in Fig. 9b, the diameter of the dowel was larger than the inner diameter of the muff (see tolerances in Table 1). Therefore, during pressing the dowel into the muff, firstly the contact pressure between surfaces of the dowel and muff were simulated, and then the mounting force increase caused by the interaction of contacting surfaces. The polyamide is modeled as elastic-perfectly plastic materials and particle board as elastic - isotropic material. In addition, geometric nonlinearity is considered to represent the large deformation of the structure. Between dowel and muff general surface contact were modeled including no friction. Computations were performed at the Poznań Supercomputing and Networking Center (PSNC) using the Eagle computing cluster. The finite element analysis was conducted using Abaqus/Explicite v.6.14-2 (Dassault Systemes Simulia Corp., Waltham, Ma, USA). The measuring point indicated in Fig. 9 was used to determine the change in the value of the contact pressures during insertion of the dowel into the muff.

On the basis of results of numerical calculations, contact pressures and coefficients of frictions of dowel joints were obtained and compared to real test results.

6. Statistical analysis

Two different approaches were applied in the statistical analyses. In the first approach, mounting force values of the reference (non-auxetic) dowels were taken into account in the analyses; thus, the mounting force differences of the 12 different auxetic dowels relative to the mounting force of reference dowels were determined. For this approach, the one-way analysis of variances (ANOVA) general linear model procedure was performed to analyze main effect (dowel type) on the mean of mounting force.

In the case of second approach, mounting force values of the reference dowels were not taken into account in the analyses. This time, effect of the two independent variables (dowel hole diameter and inclusion size) and their interaction (dowel hole diameter × inclusion size) on the mounting force were investigated. For this approach, a two-way analysis of variances (MANOVA) general linear model procedure was performed to analyze main factors and two-way interaction on the mean of mounting force.

In both cases, the least significant difference (LSD) multiple comparisons procedure at 5% significance level was performed to determine the mean differences of mounting force values of the samples tested considering the 'dowel type' that was statistically significant in the ANOVA; and 'dowel hole diameter', 'inclusion size', and 'dowel hole diameter × inclusion size' interaction that were statistically significant in the MANOVA results. Minitab (Version 17) statistical software was utilized for the statistical analyses (Minitab, LLC, State College, PA, USA).

7. Results and discussion

7.1. Auxetic properties of the dowels

In the study, auxetic properties (negative Poisson's ratio) of the designed dowels were numerically and experimentally determined. The Poisson's ratios of each designed dowel are given in Table 2.

As seen in Table 2; the Poisson's ratios calculated by numerical analyses and experimental results are on average 98% consistent with each other. For the dowels without hole (A3, A5, A7), negative Poisson's ratios were not obtained from both numerical and real tests. It means that these dowels did not show auxetic properties. From these results, it could be said that there should be hole inside the dowels for providing the auxetic properties. In the case of the dowels with hole (B3, B5, B7, C3, C5, C7, D3, D5, D7), the Poisson's ratio values of each dowel were

Table 5
Summary of MANOVA results for mounting forces according to second approach.

Source	Degrees of freedom	Sum of squares	Mean squares	F–Value	P–Value
Dowel hole diameter	3	496,520	165,507	279.53	0.000
Inclusion size	2	43,757	21,878	36.95	0.000
Hole diameter × Inclusion size	6	13,324	2221	3.75	0.002
Error	108	63,945	592		
Total	119	617,546			

Table 6
Mean comparisons for dowel hole diameter and inclusion size on mounting force.

Dowel hole diameter	Mounting force (N)		Inclusion size	Mounting force (N)	
	Mean	(HG)		Mean	(HG)
(A) 0 mm	261	A			
(B) 1.5 mm	213	B	(3) 0.3 mm	161	B
(C) 3 mm	125	C	(5) 0.5 mm	203	A
(D) 4 mm	103	D	(7) 0.7 mm	163	B

Table 7
Comparison test results for dowel hole diameter – inclusion size interaction.

Dowel hole diameter	Inclusion size					
	(3) 0.3 mm		(5) 0.5 mm		(7) 0.7 mm	
	Mean	(HG)	Mean	(HG)	Mean	(HG)
(A) 0 mm	252	B	302	A	231	BC
(B) 1.5 mm	211	CD	236	B	194	D
(C) 3 mm	96	G	151	E	127	F
(D) 4 mm	88	G	122	F	100	G

negative. This table also shows the regularity that with increasing inclusion sizes, Poisson's ratios are decreasing. Also, in the case of dowels without holes, the auxetic structure of the outer surface of the dowel causes a decrease of Poisson's ratio. Similarly, as the hole diameter in the dowel increases, the Poisson's ratio decreases.

7.2. Experimental results for mounting force

According to the first statistical approach, the ANOVA results indicated that the main factor (dowel type) for mounting force values was statistically significant at the 5% significance level on mounting forces of dowels. The results of one-way analysis of variance are given in Table 3.

Table 4 give mean comparisons of mounting force values of the dowels with their coefficients of variation values along with LSD comparison test results.

Generally, results indicated that the auxetic dowels gave lower mounting force values than the non-auxetic dowels. These results can be explained by the typical mechanical behavior of the auxetic dowels. Under the mounting force, the dowels exposed to the compression stresses in a longitudinal direction, and the diameter of auxetic dowels was getting smaller, while the diameter of non-auxetic dowels was getting larger. Therefore, auxetic dowels could insert into the muff with lower mounting force values, while non-auxetic ones could insert into the muff with higher mounting force. Dowels C3 and D7 were the easiest to insert into the muff; however, RF and A5 dowels were the most difficult to insert into the muff. Results also indicated that there was no statistically significant difference between the dowels RF and A5, A3 and B5, C3 and D3. In the case of the second approach, the MANOVA results indicated that the main factors (dowel hole diameter and inclusion size) and their interaction (dowel hole diameter × inclusion size) for mounting force values were statistically significant at the 5% significance level. Comparing the F-values to one another, it can be concluded that the mounting force was mainly affected by dowel hole diameter. The results of the two-way analysis of variance are given in Table 5.

Table 6 gives mean comparisons of mounting force values of the dowels for dowel hole diameter and inclusion size.

Results indicated that mounting force values of dowels decreased as the dowel hole diameter is increased. The mounting force of (B) dowels was lower than the mounting force of (A) dowels by 18%. In case of (C) and (D) dowels, the mounting force was considerably lower than the (A) dowels by 52% and 60%, respectively. In the case of the inclusion size, the 0.5 mm patterned dowels showed the greatest mounting force values. The mounting force values between the 0.3 and 0.7 mm patterned dowels were not statistically different. The mounting force of 0.3 and 0.7 mm patterned dowels were lower than the 0.5 mm patterned dowels on average 20%. The two-way interaction of mounting force of dowels according to the dowel hole diameter and inclusion size are given in Table 7.

As seen in Table 7; the dowels A5 had the highest mounting force values, whereas the C3, D3, and D7 dowels had the lowest. Overall, it could be said from the results; the dowels with holes that behaved auxetic properties gave lower mounting force values than the dowels without holes that behaved non-auxetic properties. According to the results, the mounting force value differences between the C7 and D5 dowels, and similarly between the A3 and B5 dowels, were not statistically significant.

7.3. Results of the numerical and theoretical calculations

The numerical and experimental load–displacement relationships of dowels under the mounting force by comparing with the reference

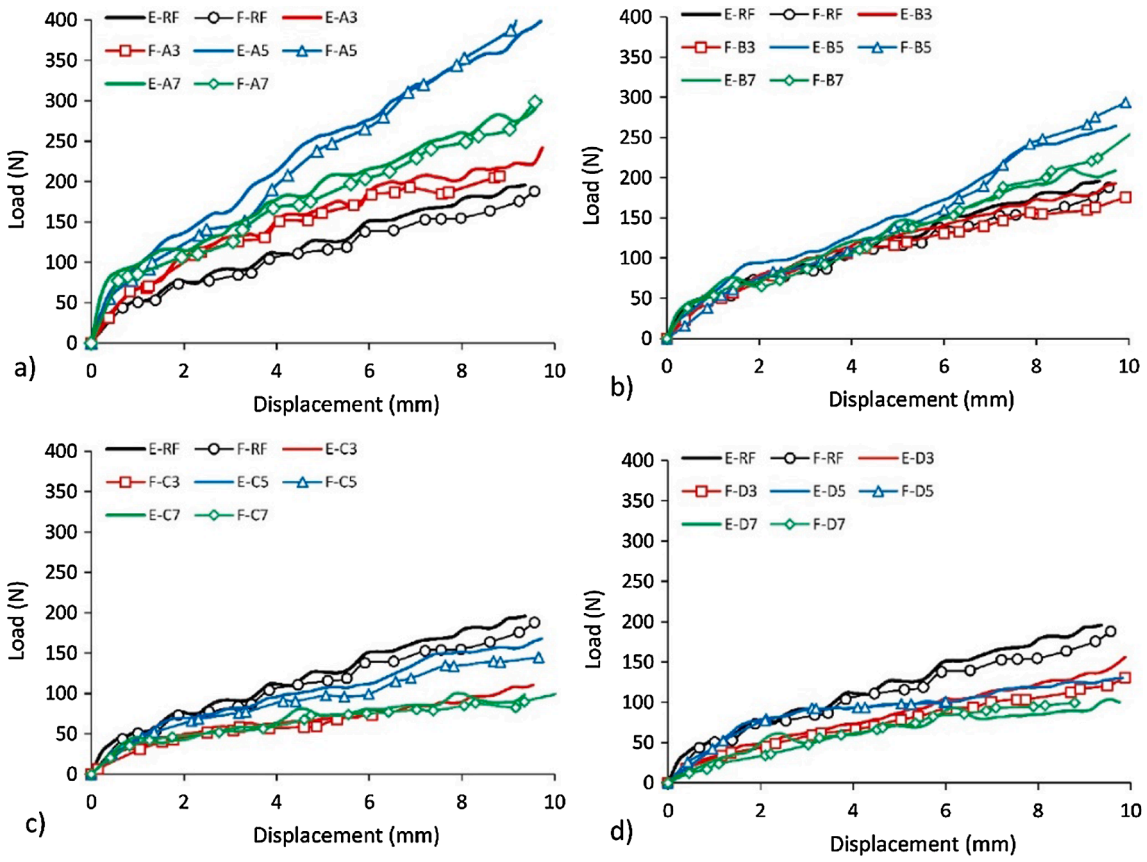

Fig. 10. Relationship between load and displacement. Comparison of the experimental (E) and numerical (F) results: (a) dowels A type, (b) dowels B type, (c) dowels C type, (d) dowels D type.

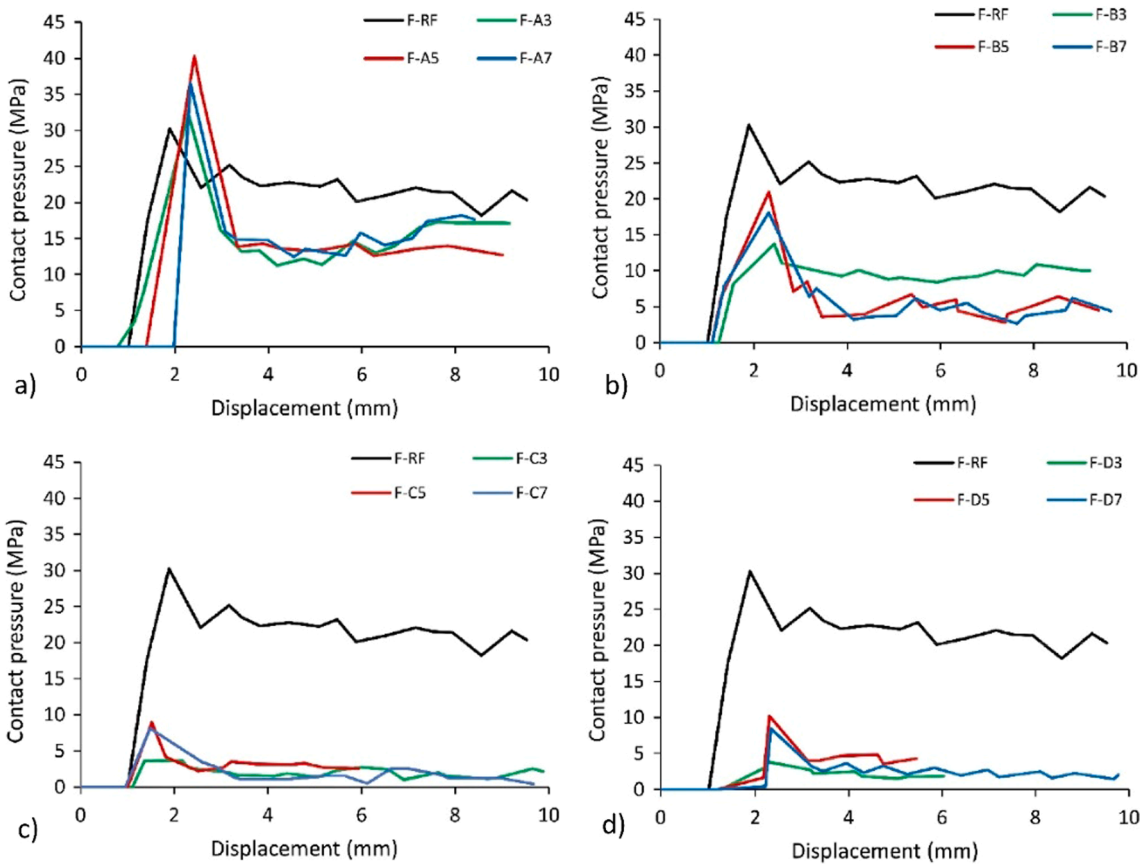

Fig. 11. Relationship between contact pressure and displacement: (a) dowels A type, (b) dowels B type, (c) dowels C type, (d) dowels D type.

dowel (RF) are given in Fig. 10 for each group. The presented comparison does not apply to average values, which were discussed in items 7.1 and 7.2, but individual selected joints from each group. In this way, it was ensured that the numerical model corresponds to a specific dowel and a specific muff. So, for this reason, the discussed maximum forces values will differ from the average values.

According to the load–displacement relations generally, the numerical (FEM) results gave reasonable estimates for the mounting force tests. It can be seen from the results that the non-auxetic dowels, without hole (A3, A5, A7), were inserted into the muff with higher mounting force values than the RF dowel. The highest mounting force was obtained from the A5 dowels among the dowels without hole. In case of the auxetic dowels has 1.5 mm diameter hole (B3, B5, B7), all dowels showed similar behavior with the RF dowel until approximately 5 mm displacement was provided. After this point, the mounting force values and mechanical behavior of the dowels were getting different. B5 dowels also gave the highest mounting force values like in the A dowel (non-auxetic) group. B5 and B7 dowels gave higher mounting force values than the RF dowel, while the B3 dowel indicated the minimum mounting force values. For the auxetic dowels has 3 mm (C3, C5, C7) and 4 mm (D3, D5, D7) diameter hole were easily inserted into the muff relative to the RF dowels. These dowels gave lower mounting force values than the RF dowels. C7 and D7 gave the lowest mounting force values among the C and D dowel groups, respectively.

Based on Fig. 10, general tendencies are also outlined. From dependence a and b, it follows that the smallest mounting forces were noted for dowel type A7, A3 and B7, B3. So, for structures with Poisson's ratio equal 0.146, 0.217, −0.237, −0.143, respectively. On the other hand, it can be seen for the c and d relationships that the smallest mounting forces were noted for dowels type C3, C7 and D3, D7. So, for structures with Poisson's ratio equal −0.185, −0.311, −0.336, −0.412, respectively. It follows that the hole diameter has a dominant effect on the reduction of mounting forces. It should be considered that increasing the diameter of the hole reduces the cross-section of the dowel and reduces its stiffness. An additional factor reducing the stiffness of the dowel joints is also the size of the inclusions. If the size of the inclusions increases, then the Poisson's ratio and the stiffness of the joints decrease. So, the overlapping of the two most unfavorable dimensional parameters causes a significant reduction in the value of mounting forces.

The contact pressures around the surface of dowels and displacement relations of dowels under the mounting force by comparing with the reference dowel were also investigated in the numerical analyses and results are given in Fig. 11 for each group.

As seen from Fig. 11, contact pressures were getting higher until

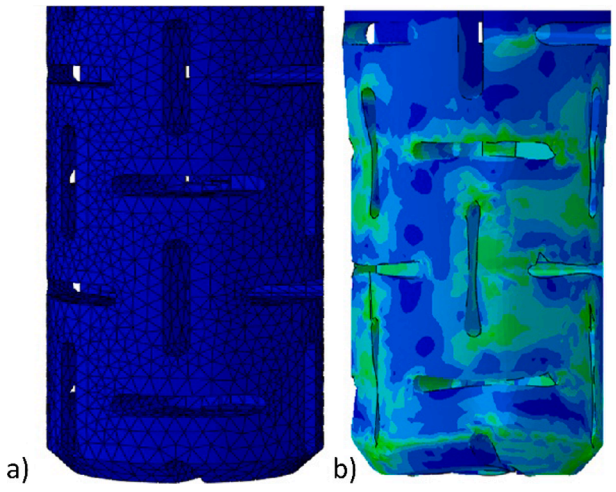

Fig. 12. Geometry of auxetic dowels before (a) and after mounting (b).

approximately 2 mm displacement was provided. After this point, the contact pressure values were getting decrease and then especially the auxetic dowels inserted into the muff under very low contact pressure values. According to the contact pressure–displacement relations; for the auxetic dowels (B3, B5, B7, C3, C5, C7, D3, D5, D7) the contact pressure values around the surface of dowels were considerably lower than the RF dowel. Contact pressures around the surface of non-auxetic dowels without hole (A3, A5, A7) were also lower than the reference dowel.

The diameter of the auxetic dowels shrunk under the mounting force because of the auxetic behavior. This phenomenon was verified by means of numerical analyses. The geometry of deflected shape of the auxetic dowel was obtained from the numerical analyses and given in Fig. 12 in comparison with the geometry of the auxetic dowel before mounting.

The Mises stress distribution inside the reference (RF) and auxetic dowels during the mounting process were obtained from the numerical analyses and the graphical results are given step by step in Fig. 13.

As seen in Fig. 13, with the effect of mounting force, the stresses inside the surface of the RF dowel decreased and increased in case of auxetic dowel as the dowel penetrated into the muff. However, the stress values inside the RF dowels were slightly higher than the auxetic dowels. During the first contact of the dowel with the muff, the largest stresses occur at the edge contact of both parts. Next, stresses increase and concentrate in the central part of the reference dowel. For the auxetic dowel, the greatest stresses occur near the inclusions. They are not greater than the maximum strength of the materials (41 MPa). Furthermore, the contact pressure distribution around the surface of reference and auxetic dowels during the mounting process were also observed from the numerical analyses and the graphical results are given in Fig. 14.

As expected contact pressure distribution around the surface of dowels gave similar tendency to the distribution of stresses around the surface of dowels. According to the numerical analyses results, contact pressure around the surface of the RF dowels decreased and increased in the case of auxetic dowel as the dowel penetrated into the muff. Fig. 14 also shows that the first highest contact pressure occurs at the edges of the muff and the dowel, i.e. at the beginning and end of the contact surface. The first contact pressures around the surface of RF dowels (36.11 MPa) were considerably higher than the auxetic dowels (19.08 MPa). In addition, in the case of the reference dowel (RF) the distribution is even, but on the surface of the auxetic dowel is concentrated near the inclusions. Therefore, the contact pressures in the auxetic dowels are significantly greater than in the RF dowels, 23.86 MPa, and 13.31 MPa, respectively.

According to the results obtained from contact pressures and stress distributions, it could be concluded that more mounting force values were required to insert the non-auxetic reference dowels into the muff than auxetic dowels.

In the study, maximum contact pressures were numerically and theoretically calculated for each dowel group and compared to each other. Theoretical calculations were performed by using the *Lame* analogy (Eqs. (8) and (11)) for the dowel with hole, and by using the classic Hook's law (Eqs. (9) and (11)) for the dowel without hole. The contact pressure values obtained from the numerical analyses and the values theoretically calculated are presented in Table 8.

As seen in Table 8, the results of calculations of contact pressures and friction coefficients differ significantly. It should be noted that for dowels RF, A (3–7) the differences between results of the FEM and Eq. (9) are much smaller than for Eq. (8). However, for auxetic dowels, the results from FEM and Eq. (8) are closer. Similar relationships were observed in the paper [55]. Therefore, taking into account the good compliance of the results of numerical calculations with the experiment, for further research, it was decided to use the results of numerical calculations.

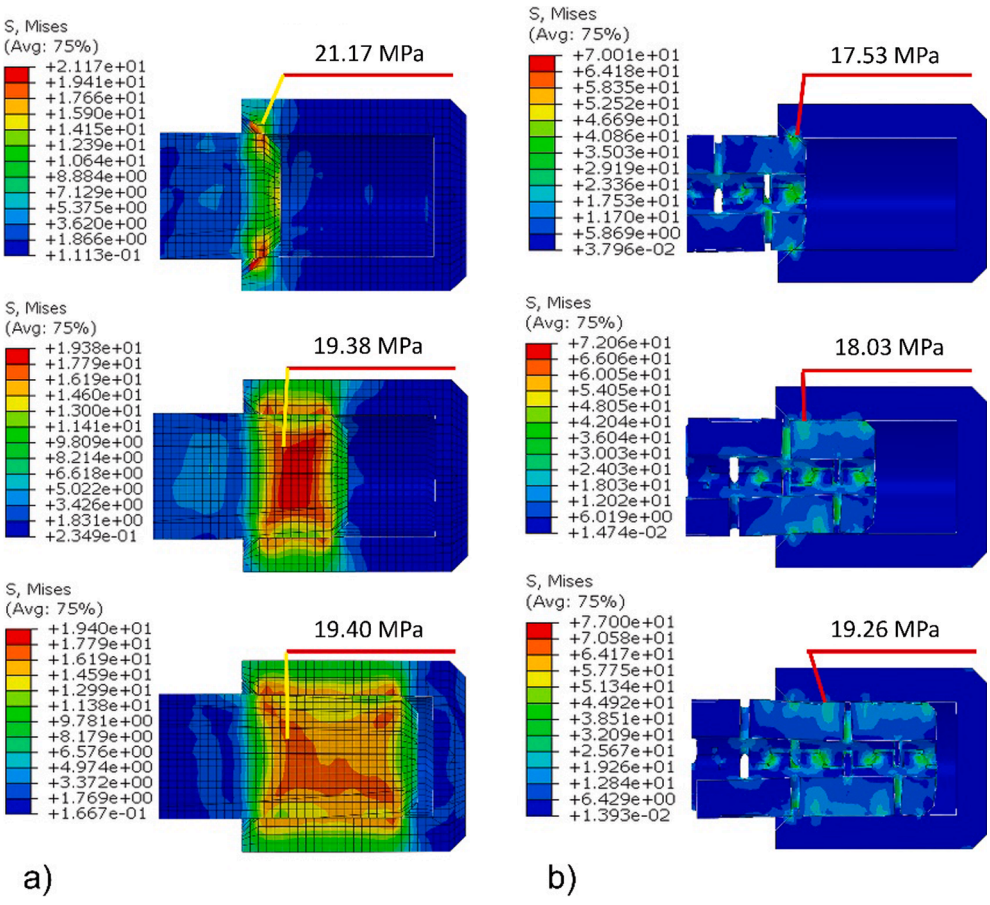

Fig. 13. Stress distribution of dowels during mounting process: (a) reference (RF) (b) auxetic.

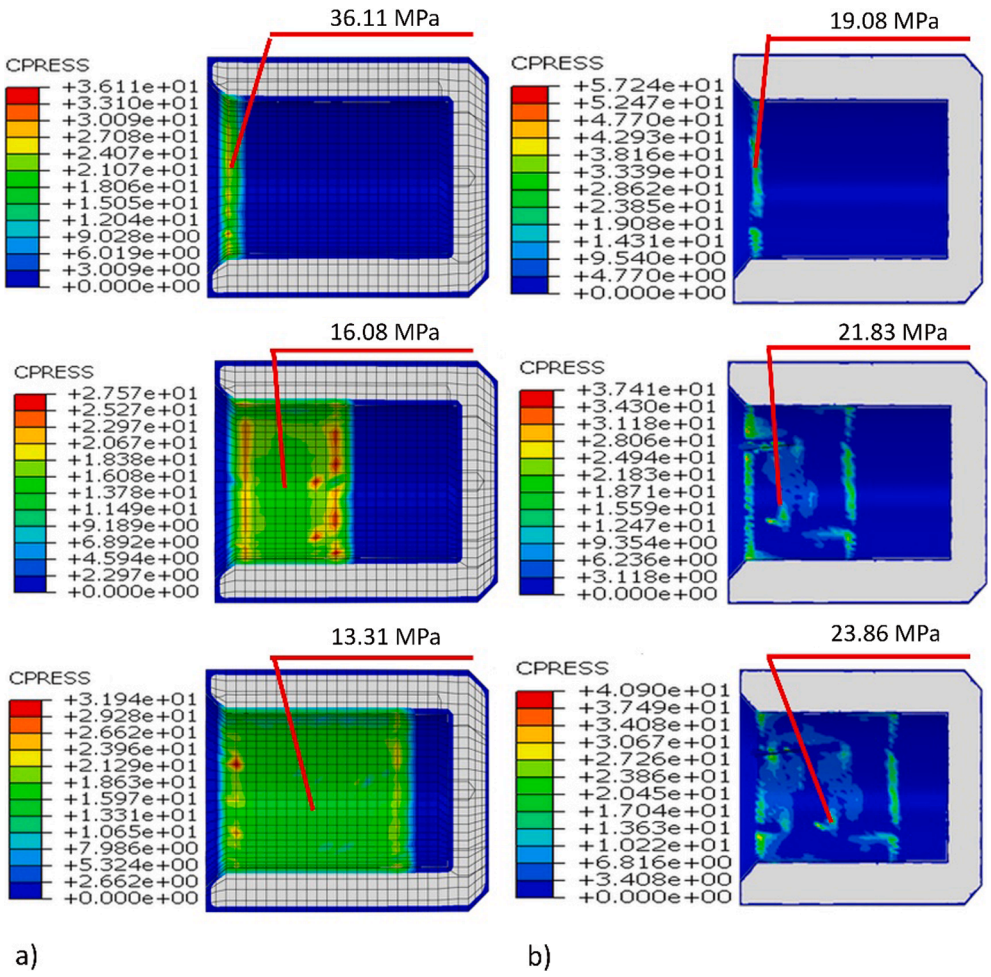

Fig. 14. Contact pressure distribution during mounting process: (a) reference (a) auxetic.

Table 8
Contact pressures and friction coefficients for the dowels.

Dowel type	Dowel code	Contact pressures (MPa)			Friction coefficients		
		FEM	Eq. (8)	Eq. (9)	FEM	Eqs. (8), (11)	Eqs. (9), (11)
Non-auxetic	RF	20.8	1.2	22.5	0.037	0.591	0.033
	A3	17.1	1.8	34.2	0.049	0.435	0.025
	A5	13.3	1.7	31.4	0.121	0.900	0.052
	A7	17.6	1.6	30.5	0.065	0.676	0.037
Auxetic	B3	10.0	1.7	33.4	0.066	0.384	0.020
	B5	2.8	1.6	31.4	0.217	0.657	0.036
	B7	4.4	1.8	35.1	0.189	0.490	0.027
	C3	1.8	1.3	28.8	0.139	0.193	0.010
	C5	2.6	1.1	25.2	0.145	0.367	0.016
	C7	1.3	1.4	31.8	0.292	0.244	0.012
	D3	1.9	1.0	27.1	0.205	0.335	0.014
	D5	3.7	0.9	23.5	0.102	0.458	0.018
	D7	1.8	1.0	27.0	0.227	0.390	0.015

8. Conclusions

This study was carried out to obtain experimental and numerical information related to the minimum mounting forces of auxetic dowels manufactured from PA12. Based on the analysis of the results of research, a couple important conclusions and suggestions could by formulated.

According to the numerical and experimental results, there should be a hole inside of the dowels for obtaining the negative Poisson's ratio. Auxetic dowels gave considerably lower mounting force values than the non-auxetic dowels. The diameter of the hole and inclusion size of auxetic dowels significantly affected the mounting force at the 5% significance level. Mounting forces of dowels decreased as the dowel hole diameter is increased. For the inclusion size between 0.3 mm and 0.7 mm, the mounting forces were not statistically different, and they gave lower mounting force than the 0.5 mm patterned dowels. According to the numerical calculations, contact pressure around the surface, and Mises stresses inside of the RF dowels were considerably higher than the auxetic dowels. Therefore, less mounting force values were required to insert the auxetic dowels into the muff. The non-auxetic A5 dowels had the highest mounting force values, whereas the auxetic C3, D3, and D7 dowels had the lowest. Results showed that numerical and theoretical analyses of the samples by FEM provide reasonable estimates of these samples consistent with the actual test results. It could be clearly seen that the numerical and experimental analyses provide useful insight into actual test results.

The results of this study provide numerical and experimental information on the mounting force of auxetic dowels, which will in turn help optimize furniture engineering design and construction of furniture joints with these kinds of fasteners. In conclusion, it was decided to continue this investigation and determine the withdrawal strength this type of dowels in furniture joints.

Declaration of Competing Interest

None.

Acknowledgements

The paper was financed also within the framework of the Ministry of Science and Higher Education programme "Regional Initiative of Excellence" in years 2019-2022, Project No. 005/RID/2018/19. This study was also supported by Scientific and Technological Research Council of Turkey (TUBITAK) under the Science Fellowships and Grant Programs with the application no. 1059B191800913. Part of the computations was performed using computers of the Poznan Supercomputing and Networking Center.

References

[1] Kolpakov AG. Determination of the average characteristics of elastic frameworks. J Appl Math Mech 1985;49:739–45. https://doi.org/10.1016/0021-8928(85)90011-5.
[2] Wojciechowski KW. Constant thermodynamic tension Monte Carlo studies of elastic properties of a two-dimensional system of hard cyclic hexamers. Mol Phys 1987;61:1247–58. https://doi.org/10.1080/00268978700101761.
[3] Cabras L, Brun M. Auxetic two-dimensional lattice with Poisson's ratio arbitrarily close to-1. ArXiv Prepr ArXiv14075679 2014:1–26. doi:10.1098/rspa.2014.0538.
[4] Lakes R. Foam structures with a negative Poisson's ratio. Science (80-) 1987;235:1038–40. doi:10.1126/science.235.4792.1038.
[5] Evans KE. Auxetic polymers: a new range of materials. Endeavour 1991;15:170–4. https://doi.org/10.1016/0160-9327(91)90123-S.
[6] Ho VH, Ho DT, Kwon S-Y, Kim SY. Negative Poisson's ratio in periodic porous graphene structures. Phys Status Solidi 2016;253:1303–9. https://doi.org/10.1002/pssb.201600061.
[7] Chen Y, Li T, Scarpa F, Wang L. Lattice metamaterials with mechanically tunable Poisson's ratio for vibration control. Phys Rev Appl 2017;7:24012. https://doi.org/10.1103/PhysRevApplied.7.024012.
[8] Lakes RS. Deformation mechanisms in negative Poisson's ratio materials: structural aspects. J Mater Sci 1991;26:2287–92. https://doi.org/10.1007/BF01130170.
[9] Milton GW. Composite materials with poisson's ratios close to — 1. J Mech Phys Solids 1992;40:1105–37. https://doi.org/10.1016/0022-5096(92)90063-8.
[10] Sigmund O. Materials with prescribed constitutive parameters: An inverse homogenization problem. Int J Solids Struct 1994;31:2313–29. https://doi.org/10.1016/0020-7683(94)90154-6.
[11] Baughman RH, Shacklette JM, Zakhidov AA, Stafström S. Negative Poisson's ratios as a common feature of cubic metals. Nature 1998;392:362–5. https://doi.org/10.1038/32842.
[12] Kimizuka H, Kaburaki H, Kogure Y. Mechanism for negative poisson ratios over the α- β transition of cristobalite, SiO2: A molecular-dynamics study. Phys Rev Lett 2000;84:5548–51. https://doi.org/10.1103/PhysRevLett.84.5548.
[13] Grima JN, Evans KE. Auxetic behavior from rotating squares. J Mater Sci Lett 2000;19:1563–5. https://doi.org/10.1023/A:1006781224002.
[14] Baughman RH. Auxetic materials: Avoiding the shrink. Nature 2003;425:667. https://doi.org/10.1038/425667a.
[15] Wojciechowski KW. Non-chiral, molecular model of negative Poisson ratio in two dimensions. J Phys A Math Gen 2003;36:11765–78. https://doi.org/10.1088/0305-4470/36/47/005.
[16] Shen J, Zhou S, Huang X, Xie YM. Simple cubic three-dimensional auxetic metamaterials. Phys Status Solidi Basic Res 2014;251:1515–22. https://doi.org/10.1002/pssb.201451304.
[17] Bertoldi K, Reis PM, Willshaw S, Mullin T. Negative Poisson's ratio behavior induced by an elastic instability. Adv Mater 2010;22:361–6. https://doi.org/10.1002/adma.200901956.
[18] Pozniak AA, Wojciechowski KW. Poisson's ratio of rectangular anti-chiral structures with size dispersion of circular nodes. Phys Status Solidi Basic Res 2014;251:367–74. https://doi.org/10.1002/pssb.201384256.
[19] Pasternak E, Shufrin I, Dyskin AV. Thermal stresses in hybrid materials with auxetic inclusions. Compos Struct 2016;138:313–21. https://doi.org/10.1016/j.compstruct.2015.11.032.
[20] Hou J, Li D, Dong L. Mechanical behaviors of hierarchical cellular structures with negative Poisson's ratio. J Mater Sci 2018;53:10209–16. https://doi.org/10.1007/s10853-018-2298-0.
[21] Narojczyk WJ, Wojciechowski WK. Poisson's ratio of the f.c.c. hard sphere crystals with periodically stacked (001)-nanolayers of hard spheres of another diameter. Materials (Basel) 2019;12. https://doi.org/10.3390/ma12050700.
[22] Airoldi A, Bettini P, Panichelli P, Oktem MF, Sala G. Chiral topologies for composite morphing structures – Part I: Development of a chiral rib for deformable airfoils. Phys Status Solidi 2015;252:1435–45. https://doi.org/10.1002/pssb.201451689.
[23] Bacigalupo A, Lepidi M, Gnecco G, Gambarotta L. Optimal design of auxetic hexachiral metamaterials with local resonators. Smart Mater Struct 2016;25:54009. https://doi.org/10.1088/0964-1726/25/5/054009.
[24] Ma Y, Scarpa F, Zhang D, Zhu B, Chen L, Hong J. A nonlinear auxetic structural vibration damper with metal rubber particles. Smart Mater Struct 2013;22:84012. https://doi.org/10.1088/0964-1726/22/8/084012.
[25] Allen T, Hewage T, Newton-Mann C, Wang W, Duncan O, Alderson A. Fabrication of auxetic foam sheets for sports applications. Phys Status Solidi 2017;254:1700596. https://doi.org/10.1002/pssb.201700596.
[26] Ren X, Shen J, Tran P, Ngo TD, Xie YM. Auxetic nail: Design and experimental study. Compos Struct 2018;184:288–98. https://doi.org/10.1016/j.compstruct.2017.10.013.
[27] Ho DT, Nguyen CT, Kwon S-Y, Kim SY. Auxeticity in metals and periodic metallic porous structures induced by elastic instabilities. Phys Status Solidi 2019;256:1800122. https://doi.org/10.1002/pssb.201800122.
[28] Alderson A, Alderson KL, Chirima G, Ravirala N, Zied KM. The in-plane linear elastic constants and out-of-plane bending of 3-coordinated ligament and cylinder-ligament honeycombs. Compos Sci Technol 2010;70:1034–41. https://doi.org/10.1016/j.compscitech.2009.07.010.
[29] Lorato A, Innocenti P, Scarpa F, Alderson A, Alderson KL, Zied KM, et al. The transverse elastic properties of chiral honeycombs. Compos Sci Technol 2010;70:1057–63. https://doi.org/10.1016/j.compscitech.2009.07.008.
[30] Imbalzano G, Tran P, Ngo TD, Lee PVS. A numerical study of auxetic composite panels under blast loadings. Compos Struct 2016;135:339–52. https://doi.org/10.1016/j.compstruct.2015.09.038.
[31] Greaves GN, Greer AL, Lakes RS, Rouxel T. Poisson's ratio and modern materials. Nat Mater 2011;10:823.
[32] Evans KE, Alderson A. Auxetic materials: functional materials and structures from lateral thinking ! Adv Mater 2000;12:617–28. https://doi.org/10.1002/(SICI)1521-4095(200005)12:9<617::AID-ADMA617>3.0.CO;2-3.
[33] Santulli C, Langella C. Study and development of concepts of auxetic structures in bio-inspired design. Int J Sustain Des 2016;3:20. https://doi.org/10.1504/ijsdes.2016.078947.
[34] Smardzewski J. Elastic properties of cellular wood panels with hexagonal and auxetic cores. Holzforschung 2013;67:87–92. https://doi.org/10.1515/hf-2012-0055.
[35] Smardzewski J, Jasińska D. Mathematical models and experimental data for HDF based sandwich panels with dual corrugated lightweight core. Holzforschung 2016;71:265–73. https://doi.org/10.1515/hf-2016-0146.
[36] Smardzewski J, Wojciechowski KW, Poźniak A. Auxetic lattice truss cores fabricated of LayWood. BioResources 2018;13:8823–38. https://doi.org/10.15376/biores.13.4.8823-8838.
[37] Smardzewski J, Wojciechowski WK. Response of wood-based sandwich beams with three-dimensional lattice core. Compos Struct 2019;216:340–9. https://doi.org/10.1016/j.compstruct.2019.03.009.
[38] Smardzewski J. Wooden sandwich panels with prismatic core – Energy absorbing capabilities. Compos Struct 2019;230:111535. https://doi.org/10.1016/j.compstruct.2019.111535.
[39] Smardzewski J. Experimental and numerical analysis of wooden sandwich panels with an auxetic core and oval cells. Mater Des 2019;183:108159. https://doi.org/10.1016/j.matdes.2019.108159.
[40] Smardzewski J, Klos R, Fabisiak B. Design of small auxetic springs for furniture. Mater Des 2013;51:723–8. https://doi.org/10.1016/j.matdes.2013.04.075.
[41] Smardzewski J. Auxetic springs for seating. Turkish J Agric For 2013;37:369–76. https://doi.org/10.3906/tar-1204-64.
[42] Uysal B. Withdrawal strength of various laminated veneer dowels from composite materials. Wood Fiber Sci 2005;37:213–9.
[43] Erdil YZ, Zhang J, Eckelman CA. Withdrawal and bending strength of dowel-nuts in plywood and oriented strandboard. For Prod J 2003;53:54–7.
[44] Cha JK. The effect of diameter and prehole clearance for wooden dowel on the withdrawal loads of domestic wood. J Korean Wood Sci Technol 2016;44:736–42. https://doi.org/10.5658/WOOD.2016.44.5.736.
[45] Yapici F, Likos E, Ras E. The effect of edge banding thickness of some trees on withdrawal strength of beech dowel pins in composite material. Wood Res 2011;56:601–12.
[46] Özcan C, Uysal B, Kurt Ş, Esen R. Effect of dowels and adhesive types on withdrawal strength in particleboard and MDF. J Adhes Sci Technol 2013;27:843–54. https://doi.org/10.1080/01694243.2012.727157.
[47] Eckelman C, Cassens D. Withdrawal strength of dowels from wood composites. For Prod J 1985;35:55–60.
[48] Erdil ZY, Eckelman CA. Withdrawal strength of dowels in plywood and oriented strand board. Turk J Agric 2001;25:319–27.
[49] Hao J, Xu L, Wu X, Li X. Analysis and modeling of the dowel connection in wood T type joint for optimal performance. Compos Struct 2020;253:112754. https://doi.org/10.1016/j.compstruct.2020.112754.
[50] ASTM International. ASTM D3039 / D3039M - 17 Standard Test Method for Tensile Properties of Polymer Matrix Composite Materials. 2017. doi:10.1520/D3039_D3039M-17.
[51] Peliński K, Smardzewski J. Experimental testing of elastic properties of paper and WoodEpox® in honeycomb panels. BioResources 2019;14:2977–94. https://doi.org/10.15376/biores.14.2.2977-2994.
[52] Maslej M, Smardzewski J. Experimental testing of elastic properties of LayWood pyramidal cores. BioResources 2019;14:9686–703. https://doi.org/10.15376/biores.14.4.9686-9703.
[53] Słonina M, Dziurka D, Smardzewski J. Experimental research and numerical analysis of the elastic properties of paper cell cores before and after impregnation. Materials (Basel) 2020;13:2058. https://doi.org/10.3390/MA13092058.
[54] Lipka J. Wytrzymałość maszyn wirnikowych. Warszawa: WNT; 1967.
[55] Madej J. A strength analysis of the interference-fit joints. Mechanik 2018;91:1032–4. https://doi.org/10.17814/mechanik.2018.11.185.